# COMPUTATIONAL IMAGING SYSTEMS FOR THE INFRARED: REVOLUTION OR EVOLUTION?

OECD CONFERENCE CENTER, PARIS, FRANCE / 8–10 FEBRUARY 2012

**Andrew Wood[(1)], Nicholas Bustin[(1)] and Gonzalo Muyo[(2)]**

*[(1)]Qioptiq Ltd, Glascoed Road, St. Asaph, Denbighshire, UK, LL17 0LL*
*Email: andy.wood@uk.qioptiq.com; Tel: +44 (0)1745 588291*

*[(2)]Heriot-Watt University, Riccarton, Edinburgh, UK, EH14 4AS*
*Email: g.muyo@hw.ac.uk*

**KEYWORDS:** Infrared, computational imaging, wavefront coding, multi-aperture, multi-scale.

## ABSTRACT

Computational imaging techniques represent a potentially disruptive technology which can remove some of the fundamental rules determining the minimum size, weight and cost of imaging systems using conventional optics. The validity of this statement is verified using three distinctly different techniques applied to state-of-the-art infrared optical systems for uncooled sensor arrays. The design examples described show that significant benefits can be achieved in terms of system complexity, overall length and total field coverage.

## 1. INTRODUCTION

Market drivers for many applications of infrared optical systems are dominated by an ever increasing demand to reduce size, weight and cost whilst maintaining an acceptable level of image quality. In order to meet this demand, significant advances in materials and manufacturing technologies have evolved over the past few decades. Lens element count is minimised by the use of increasingly extreme aspheric forms on a greater number of surfaces, by employing hybrid refractive-diffractive components, and through the availability of new materials. Cost can be further reduced by moulding finished lenses.

These technologies enable the correction of aberrations with a minimum number of lens elements which can subsequently be manufactured using cost-effective processes. However, despite these significant advances, the size, weight and cost of conventional optical solutions is ultimately dominated by the first order properties of the system such as focal length, field-of-view and aperture diameter. Requirements to accommodate a large range of object distances, to provide multiple fields-of-view or to operate over multiple spectral ranges add complexity to the opto-mechanical solution, which conventional technologies can only mitigate to a limited extent.

Computational imaging combines novel optical solutions with digital image processing and offers the potential to challenge and break some of the current rules which determine the minimum size, weight and cost which are achievable for a given application. In this paper we discuss a number of techniques and evaluate their potential impact on future infrared systems. A key objective of our current work is to understand whether this new approach is simply another tool in the optical designer's tool box, or a significant disruptive technology.

Following a brief review of the current state-of-the art of infrared optics for uncooled sensors, we shall illustrate the potential benefits and weaknesses of three distinct computational imaging techniques by describing specific design examples. The techniques are wavefront coding, multi-aperture systems and multi-scale optics.

## 2. CURRENT STATE-OF-THE-ART

Reference [1] provides a detailed overview of the design methodology and enabling technologies in infrared optics designed to minimise size, weight and cost. Two-element lenses utilising multiple aspheric and diffractive surfaces provide a valuable insight into the current state-of-the-art. It is now commonplace for the number of non-spherical surfaces to exceed the number of lens elements, providing the degrees of freedom necessary to correct aberrations to the required level. The use of non-spherical surfaces is also an important factor in controlling the sensitivity of the lens to manufacturing tolerances, a crucial factor in the development of cost-effective products. Aspheric and diffractive surfaces also enable a greater range of optical materials to be employed, providing the capability to design passively

athermalised solutions without the need for additional lens elements. Future applications will employ multi-spectral optics to take advantage of current developments in detector technology. Innovative use of aspheric components and appropriate materials can create very simple solutions for these emerging applications.

Whilst fixed-focus operation is possible for some applications, determined by a sufficiently short focal length and large depth of focus, many systems require a focus mechanism. This can result in significant additional complexity in the mechanical construction, adding further cost and mass. In addition, focus mechanisms can adversely affect both boresight stability, critical to some applications, and reliability. Wavefront coding is a computational imaging technique with the potential to eliminate the need for a focus mechanism, as discussed in section 3.

Whilst the power construction of the system (e.g. Petzval, telephoto, inverse telephoto) has a fundamental effect on the overall length of the lens, it is parameters such as focal length, field-of-view and F-number which ultimately determine the minimum size which can be achieved using traditional optics. However, two computational imaging techniques have been investigated which break the limitations set by the first-order properties of the lens, providing opportunities to reduce size beyond that which can ever be achieved with conventional optics. Design examples using multi-aperture imaging and multi-scale optics are described in sections 4 and 5 respectively.

## 3. WAVEFRONT CODING

Phase encoded imaging is a technique in which the phase of the transmitted wavefront is manipulated to provide imaging performance parameters with particular desirable properties. Wavefront coding is a specific example of this generic technique, in which the pupil phase is modified to generate a point spread function (PSF) which is invariant with image-plane defocus [2]. Reference [1], section 7, discusses a modification to a two-element infrared lens which uses wavefront coding to extend the depth-of-field sufficiently to avoid the need for a focus mechanism. The first-order limitation in which depth-of-focus is proportional to the wavelength and $(\text{F-number})^2$ can be broken with this technique. The only change to the optics in this particular implementation is the replacement of a conventional aspheric surface with one of non-rotationally symmetric form. Such a surface is readily manufactured by current diamond turning technology.

A wavefront coded lens produces a modulation transfer function (MTF) which is suppressed compared with that of a well-corrected lens, but remains constant over an extended depth-of-focus. In addition, the MTF contains no zeros over the spatial frequency range of interest and can be restored using a single deconvolution-type algorithm in post-detector image processing. However, boosting MTF in this way also results in amplification of the detector noise, which degrades image quality. Dependent on the form of wavefront coding surface, artefacts can also be introduced into the restored image.

In general, larger depth-of-focus extensions result in greater noise amplification but less pronounced image artefacts. The optimisation of the system, by varying the wavefront coding surface shape and reconstruction algorithm parameters, becomes a complex problem which is outside the capability of conventional optical design software. We have addressed this problem by the development of specialist design software which uses image based measures such as the Root Mean Square Error (RMSE) as the performance metric [3, 4]. Such an approach is necessary to achieve the optimum trade-off between depth-of-focus increase and image quality.

In order to validate our design software, evaluate the potential value of wavefront coding to infrared imagers and make comparisons with conventional lens solutions, we have developed a demonstrator camera. The hardware incorporates an optical system with a diamond turned surface of trefoil form on one of the lenses, uncooled infrared camera and an implementation of the image processing algorithm running in real-time in low power electronics [5].

Captured images from this wavefront coding demonstrator system, compared with an equivalent conventional lens focused at 20 m, are shown in Figure 1. Two alternative forms of image processing algorithms have been implemented; these are Wiener and Constrained Least Squares (CLS) filtering. The images demonstrate increased depth-of-field for the wavefront coding system combined with increased noise which is dependant on the form of image processing algorithm. Evidence of artefacts is also present in the restored scenes.


*Figure 1. Captured images comparing similar scenes for conventional system focused at 20 m, wavefront coding system using Wiener algorithm and wavefront coding system using CLS algorithm*

Removal of a focus mechanism is not the only potential benefit which wavefront coding can provide in infrared systems; the technique can be used to mitigate the detrimental effects of any defocus-like aberration. Therefore, the technique can potentially be used for athermalisation [6] or to accommodate broad spectral bands, whilst avoiding the use of less desirable materials. Sensitivity to some lens manufacturing tolerances (e.g. surface radii, lens thickness and separation) can be reduced and time consuming focus setting may be avoided during final assembly; these factors can have a significant impact on product cost. For some applications, wavefront coding can enable a single lens solution to provide acceptable imagery over an extended field-of-view [7].

## 4. MULTI-APERTURE IMAGING

Multi-aperture imagers employ multiple parallel shorter-focal-length imaging lenses in place of a conventional single longer-focal-length lens to produce a set of low-resolution images that are computationally fused to produce a single high-resolution image [8]. The technique relies on aliasing to encode high spatial frequency information and disparity between the recorded images to enable super-resolution algorithms to reconstruct a high resolution image. By employing an array of shorter focal length imagers it is possible to significantly reduce the length of the imaging system without yielding resolution.

### 4.1. Optical design

The aim is to produce a smaller and lighter multi-aperture imaging system whilst providing a similar resolution performance to a larger conventional single-aperture lens. The baseline conventional design is a two-element infrared Petzval lens for the long-wave infrared (LWIR) with focal length of 114 mm, operating at F/1.6 over a full field-of-view of 8°. The overall length of this system is around 125 mm, with a diameter 71 mm.

The equivalent LWIR multi-aperture imaging system consists of a 3x3 array of imaging channels, as shown in Figure 2. Each channel provides a field-of-view of 8°, common to all channels, and is composed of two germanium elements resulting in an F/1.6 optical system with a nominal focal length of 38 mm.

For simplicity, we assume a square sensor with 640x640 pixels and a 25 μm pixel pitch. The Nyquist frequency is 20 cycles/mm. The system is 45 mm long, a factor of almost three shorter than the conventional baseline lens, and a similar width of 72 mm.

After optimisation of the wavefront error between the 8 to 12 µm wavelength range, the performance of the imaging channels is virtually diffraction limited. The system has been designed to operate at infinite conjugates. As an illustration, the MTF for the imaging channels situated at the centre and corners of the array are displayed in Figures 3 and 4 respectively.

Thus, given the input scene shown in Figure 5, this system produces nine under sampled images with diffraction limited performance. A simulation of the full sensor frame acquired by the system is displayed in Figure 6. Note that the acquisition of non-redundant information across the channels is enabled by the different geometric distortions that vary from channel to channel. To prevent overlap between adjacent images and cross talk, the system will contain a series of field stops and baffles that limit the field of view of each channel and block any light that crosses from one channel into another.

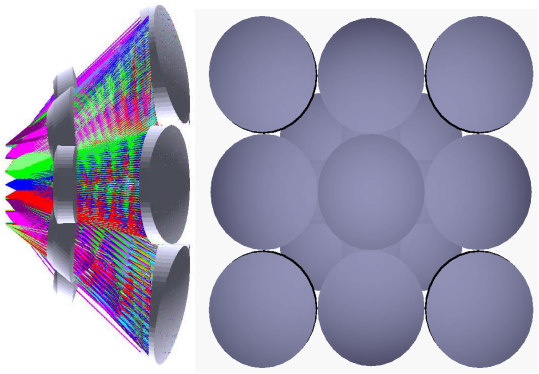

*Figure 2. Side and font view of the multi-aperture system*

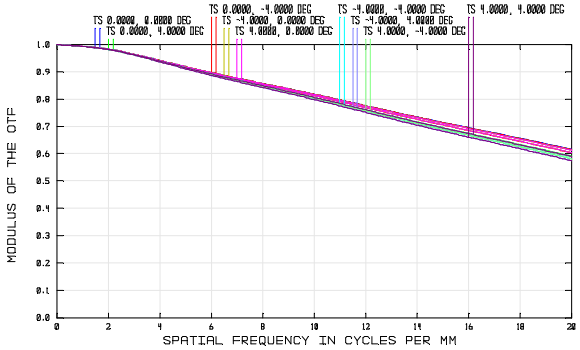


*Figure 3. Central channel MTF for various FOV's up to the Nyquist frequency*

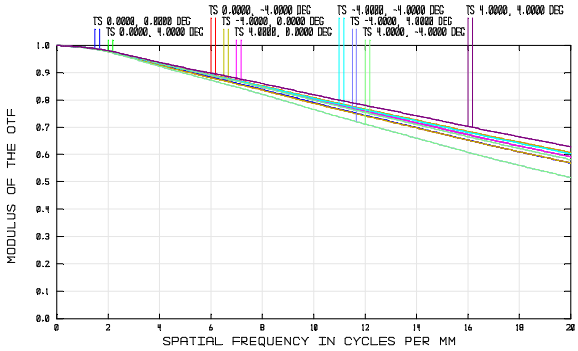


*Figure 4. Corner channel MTF for various FOV's up to the Nyquist frequency*

*Figure 5. High resolution scene (original image courtesy of Sierra Pacific Innovations Corp [www.x20.org](http://www.x20.org))*

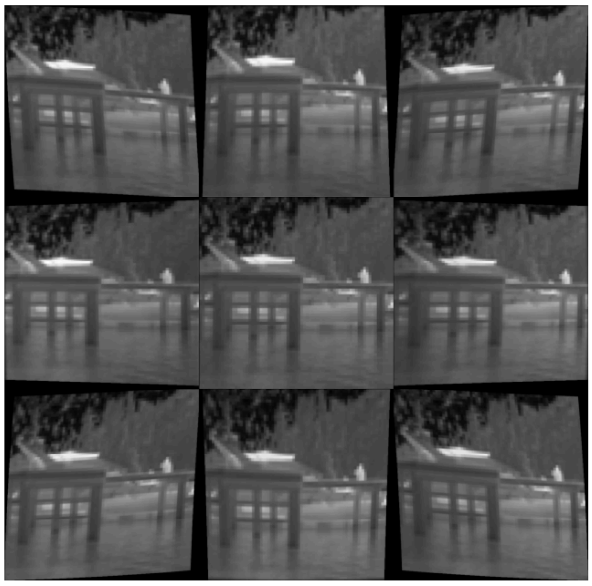

*Figure 6. Full frame acquired with the multi-aperture system (detected frame has been rotated for display)*

### 4.2. Image Processing

Fundamentally, the reconstruction process fuses the set of low-resolution under sampled images to produce a single high-resolution image. The super-resolution reconstruction is a well known problem and has been extensively studied in the literature; for a technical overview see [9].

The super-resolution model describes the relationship between the acquired *N* low-resolution images, denoted by $\mathbf{y}_k$, and the high-resolution scene $\mathbf{x}$ and can be formulated in matrix notation as [10, 11]:

$$\mathbf{y}_k = \mathbf{D}_k\mathbf{H}_k\mathbf{W}_k\mathbf{x} + \mathbf{e}_k \quad \text{for } 1 \le k \le N \tag{1}$$

where $\mathbf{W}_k$ is a matrix representing the distortion or warping operator between $\mathbf{x}$ and the $k^{th}$ image $\mathbf{y}_k$, $\mathbf{H}_k$ is the blur matrix representing the space variant point-spread function across the sensor, and $\mathbf{D}_k$ is the decimation matrix representing the sampling operator that reduces the resolution in the acquired images. The vector $\mathbf{e}_k$ stands for the additive noise in the $k^{th}$ image $\mathbf{y}_k$. In the system presented here, the size of the nine images is 213x213 pixels which are subsequently fused to produce a 639x639 high-resolution image.

By grouping the matrices in Eq. (1) into one matrix $\mathbf{F}$, with

$$\mathbf{F} = \begin{bmatrix} \mathbf{F}_1 \\ \mathbf{F}_2 \\ \vdots \\ \mathbf{F}_N \end{bmatrix} = \begin{bmatrix} \mathbf{D}_1\mathbf{H}_1\mathbf{W}_1 \\ \mathbf{D}_2\mathbf{H}_2\mathbf{W}_2 \\ \vdots \\ \mathbf{D}_9\mathbf{H}_9\mathbf{W}_9 \end{bmatrix}, \tag{2}$$

the imaging model can be expressed as:

$$\mathbf{y} = \mathbf{F}\mathbf{x} + \mathbf{e}\,, \tag{3}$$

which shows that the super-resolution problem can be treated as a classic inverse problem in which an estimate of $\mathbf{x}$ can be recovered from prior knowledge of the linear operator $\mathbf{F}$ (i.e. image distortion, shift-variant PSFs and the sampling characteristic of the sensor). Matrix $\mathbf{F}$ can be obtained from data calculated in a conventional ray tracing software tool, such as Zemax, or through a calibration process once the imaging system is constructed.

Many reconstruction algorithms assuming different noise models have been employed in the literature for the solution of this inverse problem [9 - 12]. In this work, the noise in the acquired images is modelled as Poisson noise and the reconstruction algorithm is based on the maximum likelihood approach [13]. Future work will explore the use of other reconstruction algorithms assuming different types of noise such as Gaussian noise.

The reconstruction algorithm is an iterative method in which $\mathbf{x}_n$ denotes the current estimate and $\mathbf{x}_{n+1}$ the new estimate as defined by:

$$\mathbf{x}_{n+1} = \mathbf{x}_n \left( \mathbf{F}^T \frac{\mathbf{y}}{\mathbf{F}\mathbf{x}_n} \right) \tag{4}$$

thus each step in the new estimate $\mathbf{x}_{n+1}$ is an improvement over the old estimate $\mathbf{x}_n$ (in the maximum likelihood sense).

(a) (b) (c)

*Figure 7. (a) Detail of the low-resolution image corresponding to central channel; (b) Detail of reconstructed high-resolution image (c) Detail of scene. Images acquired with SNR=100.*

The infrared scene consisting of a docked boat and a person in Figure 5 is imaged by the multi-aperture system with mean a signal-to-noise ratio (SNR) of 100. The 213×213 pixel sub-image from the central channel is shown in Figure 7(a), note the presence of aliasing artefacts. The high-resolution image iteratively restored using all low-resolution sub-images is shown in Figure 7(b). Clearly, the reconstruction algorithm has been able to recover a spatial resolution similar to the original high resolution scene; see Figure 7(c).

## 5. MULTI-SCALE IMAGING

In the original concept proposed by Brady et al. [14], multi-scale imaging is a design approach that aims to break the relationships between geometric aberrations, lens complexity and aperture size which govern the design of traditional optical systems [15]. In multi-scale imaging, the field-of-view is increased by concatenating additional lens arrays that correct aberrations *locally* and produce overlapping partial images which are subsequently processed to create a single image with wide field coverage [16, 17].

The work presented here is inspired by the original concept of multi-scale imaging. However, in contrast to the original approach, our design contains no intermediate image planes and, as a result, is required to accommodate more severe overlaps in the partial images.

### 5.1. Optical design

The LWIR system consists of a rotationally symmetric meniscus front element and rear element containing an array of 13 lenslets, as shown in Figure 8. All elements are made from germanium. The full field-of-view is 72°. Unlike other multi-scale designs that use multiple sensors distributed on a spherical arrangement [17], our system employs only one sensor. The detector is assumed to have 640x640 pixels with a 25 µm pixel pitch. In this design, each lenslet in the second optical element corrects aberrations in a small localised region of the field-of-view. Thus, for a given field point, the wavefront may be partitioned into several segments, resulting in multiple separated PSF's in the focal plane.

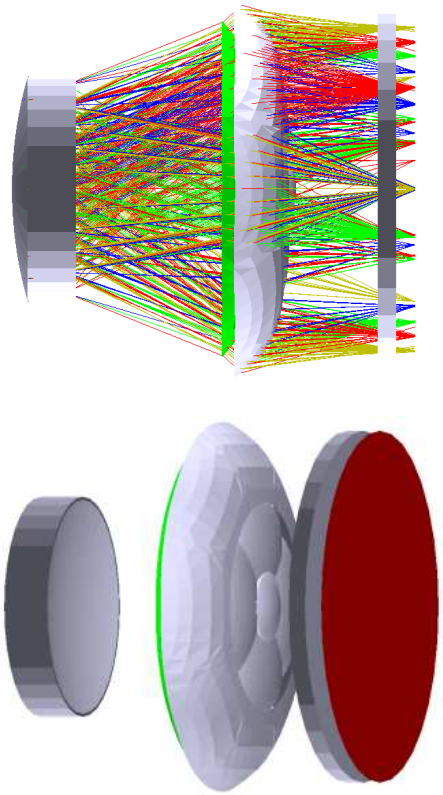

*Figure 8. Layout of the multi-scale imaging system. The red surface corresponds to the sensor.*

The imaging performance has been optimised with constrains which penalise abrupt surface transitions between lenslet boundaries. The MTF's for the three lenslets replicated across the lenslet array are shown in Figure 9. An illustration of the type of image acquired with this system is shown in Figure 10; the image is simulated with additive Poisson noise with mean SNR of 100.

The development of this multi-scale solution started with a conventional two-element baseline lens, of similar length and overall diameter, designed to provide a total field-of-view of 12° for the same sensor. The goal was to increase the field coverage without increasing lens complexity or size and mass of the optical system. With conventional lenses, the total field coverage could not be pushed beyond 20° whilst maintaining the above constraints.

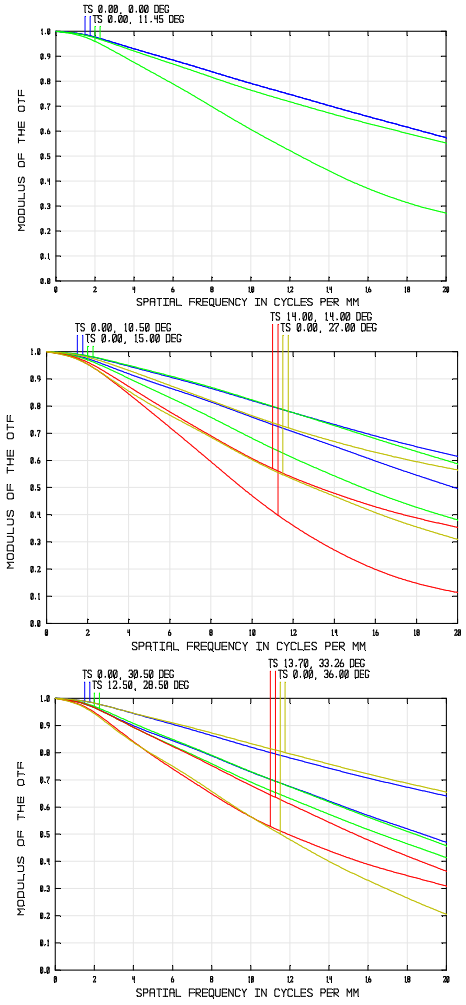


*Figure 9. MTF's up to the Nyquist frequency for the three lenslets and various FoV's.*

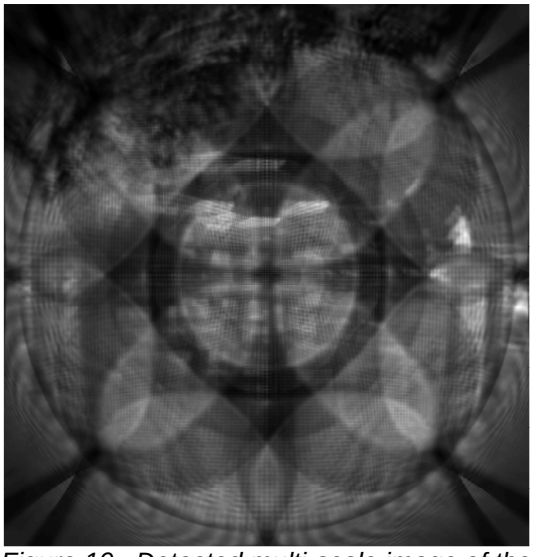

*Figure 10. Detected multi-scale image of the docked boat and person shown in Figure (mean SNR=100).*

### 5.2. Image Processing

The imaging process in the multi-scale system can be described by the linear forward model:

$$\mathbf{y} = \mathbf{F}\mathbf{x} + \mathbf{e} \qquad (5)$$

where **y** is the detected image, **x** is the scene, **e** is the noise and **F** is the linear space-variant blur matrix representing the PSF for every point on the image plane. The matrix **F** also contains information on the geometric transformation between the object and image spaces. The acquired image **y** is restored using the same iterative algorithm described in Eq.(4). Simulations of the restored image is shown in Fig.5. The images have been acquired with a mean SNR of 100 and Poisson noise statistics.

*Figure 11. Restored multi-scale image (SNR=100) with a field of view of 72°*

### 6. CONCLUSIONS

We have shown that computational imaging techniques can be used to break some of the fundamental rules which determine the limitations on size, weight and cost of conventional optical systems. Specific examples of uncooled objective lenses for operation in the LWIR spectral region have been used to highlight the potential benefits.

Wavefront coding can be used to significantly increase the depth-of-focus limitation governed by the F-number and operating wavelength of a conventional lens. The image processing can be implemented to run in real-time and remove the need for a focus mechanism. However, trade-offs

between the increased depth-of-focus, imaging artefacts and noise amplification must be carefully managed, requiring specialised optimisation strategies to be developed.

We have designed a multiple aperture system which is a factor of two-and-a-half times shorter than the focal length of a conventional lens providing equivalent resolution. It uses the same number of optical elements as the conventional baseline design and is contained within a similar diameter.

A new interpretation of the multi-scale optics concept has been presented. We have designed a two-element system with a total field coverage of at least a factor of three greater than could be achieved with a conventional lens of the same level of complexity and overall size.

The reader is left to ponder the question, is computational imaging simply a new tool in the optical engineer's toolbox, or does it represent a significant disruptive technology?

## 7. REFERENCES


[1] Bigwood, C. and Wood, A. (2011), Two-element lenses for military applications, *Opt. Eng.*, Vol. 50, No. 12, 121705.

[2]. Dowski, E. R. and Cathey, W. T. (1995), Extended depth of field through wavefront coding, *Appl. Opt.*, Vol. 34, No. 11, pp 1859 – 1866.

[3] Vettenburg, T., Wood, A., Bustin, N. and Harvey, A. (2010), Fidelity comparison of phase masks for hybrid imaging, *Proc. SPIE*, Vol. 7652, 76520U.

[4] Vettenburg, T., Bustin, N. and Harvey, A. (2010), Fidelity optimisation for aberration-tolerant hybrid imaging systems, *Opt. Express*, Vol. 18, No. 9, p 9220 – 9228.

[5] Hasler, I., Bustin, N. and Price, D. (2010), Thermal imaging system using optimised wavefront coding operating in real-time, *Proc. SPIE*, Vol. 7834, 783402.

[6] Muyo, G. and Harvey, A. (2004), Wavefront coding for athermalisation of infrared imaging systems, *Proc. SPIE*, Vol. 5612, pp 227 – 235.

[7] Muyo, G., Singh, A., Andersson, M., Huckridge, D., Wood, A. and Harvey, A. (2009), Infrared imaging with a wavefront-coded singlet lens, *Opt. Express*, Vol. 17, No. 23, pp 21118 – 21123.

[8] Tanida, J., Kumagai, T., Yamada, K., Miyatake, S., Ishida, K., Marimoto, T., Kondou, N., Miyazaki, D. and Ichioka, Y. (2001), Thin observation module by bound optics (TOMBO): concept and experimental verification, *Appl. Opt*., Vol. 40, No. 11, pp 1806-1813.

[9] Park, S. C., Park, M. K. and Kang, M. G. (2003), Super-resolution image reconstruction: a technical overview, *IEEE Signal Processing Magazine*, Vol. 20, No. 3, pp 21–36.

[10] Elad, M. and Feuer, A. (1997), Restoration of a single super resolution image from several blurred, noisy, and under sampled measured images, , *IEEE Transactions on Image Processing*, Vol. 6, No.12, pp.1646 - 1658.

[11] Farsiu, S., Robinson, M. D., Elad, M. and Milanfar, P. (2004), Fast and robust multi-frame super-resolution, *IEEE Transactions on Image Processing*, Vol. 13, No. 10, pp 1327-1344.

[12] Shankar, M., Willett, R., Pitsianis, N., Schulz, T., Gibbons, R., Te Kolste, R., Carriere, J., Chen, C., Prather, D. and Brady, D. (2008), Thin infrared imaging systems through multi-channel sampling, *Appl. Opt*., Vol. 47, No. 10, pp B1-B10.

[13] Shepp, L. A. and Vardi, Y. (1982), Maximum likelihood reconstruction for emission tomography, *IEEE Transactions on Medical Imaging*, Vol. 1, No. 2, pp 113 - 122.

[14] Brady, D. J. and Hagen, N. (2009), Multi-scale lens design, *Opt. Express*, Vol. 17, No. 13, pp 10659 - 10674.

[15] Lohmann, A. W. (1989), Scaling laws for lens systems, *Appl. Opt*., Vol. 28, No. 23, pp 4996 – 4998.

[16] Marks, D. L., Tremblay, E. J., Ford, J. E. and Brady, D. J. (2011), Microcamera aperture scale in monocentric gigapixel cameras," *Appl. Opt*., Vol. 50, No. 30, pp 5824 - 5833.

[17] Son, H., Marks, D. L., Tremblay, E. J., Ford, J., Hahn, J., Stack, R., Johnson, A., McLaughlin, P., Shaw, J., Kim, J. and Brady, D. J. (2011), A multi-scale, wide field, gigapixel camera, *Imaging Systems Applications: OSA Technical Digest*, JTuE2.